Published in final edited form as:
J Photochem Photobiol A Chem. 2008 December 15; 200(2-3): 346–355. doi:10.1016/j.jphotochem.2008.08.006.

Photophysical Characterization of Imidazolium-Substituted Pd(II), In(III), and Zn(II) Porphyrins as Photosensitizers for Photodynamic Therapy

Hooi Ling Kee[1], **Jayeeta Bhaumik**[2], **James R. Diers**[3], **Pawel Mroz**[4,5], **Michael R. Hamblin**[4,5,6], **David F. Bocian**[3], **Jonathan S. Lindsey**[2], and **Dewey Holten**[1,*]

[1] Department of Chemistry, Washington University, St. Louis, MO 63130-4889

[2] Department of Chemistry, North Carolina State University, Raleigh, NC 27695-8204

[3] Department of Chemistry, University of California, Riverside, Riverside, CA 92521-0403

[4] Wellman Center for Photomedicine, Massachusetts General Hospital, Boston, MA 02114

[5] Department of Dermatology, Harvard Medical School, Boston, MA 02115

[6] Harvard-MIT Division of Health Sciences and Technology, Cambridge, MA 02139

1. Introduction

Photodynamic therapy (PDT) is emerging as an important treatment for many diseases. Many applications of PDT involve killing undesirable disease-causing cells such as malignant cancer cells [1] or pathogenic microorganisms [2]. PDT is also used to destroy unwanted tissues such as tumors [3], new blood vessels [4], and atherosclerotic plaques [5]. The therapy involves the use of a dye or photosensitizer molecule that should localize in the target tissue, cell, or organelle, and which then leads to the formation of lethal reactive oxygen species upon light activation in the presence of molecular oxygen [6]. The photosensitizer should have a long-lived triplet excited state that allows formation of reactive oxygen species by processes such as energy transfer from the photosensitizer to ground state oxygen to form singlet excited-state oxygen (Type II mechanism), or electron transfer from the photosensitizer to ground state oxygen to form superoxide radical anion and species therefrom such as oxygen radicals (Type I mechanism) [7].

Many photosensitizers are tetrapyrrole chromophores, which includes porphyrins, chlorins, bacteriochlorins, benzoporphyrins, and phthalocyanines [8]. Many of the clinically employed photosensitizers are porphyrins, which have only weak absorption bands in the red region of the spectrum where light has the ability to penetrate tissue. Newer photosensitizers under investigation and development have much higher absorption at red and near-infrared wavelengths, where absorption by hemoglobin and other endogenous species is diminished. The four nitrogen atoms of the tetrapyrrole macrocycle efficiently chelate a variety of metal ions, and the chelated metal modulates some of the important photophysical parameters that affect the formation of the reactive oxygen species. Most naturally occurring tetrapyrrole

*Corresponding author. Tel.: +1 314 935 6502; Fax: +1 314 935 4481. Email address: holten@wustl.edu.

compounds are metal chelates; for example, the heme cofactors of hemoglobin and cytochromes are Fe(II) porphyrins, while chlorophyll or bacteriochlorophyll is a Mg(II) chlorin or bacteriochlorin, respectively.

A range of seemingly disparate tetrapyrrole structures containing metal chelates have been investigated as photosensitizers in clinical applications. Zinc(II) and aluminum(III) phthalocyanines have been studied as both unsubstituted compounds [9] and with varying numbers of sulfonated groups attached to the benzo substituents [10]. Silicon(IV) is chelated in the phthalocyanine known as PC4 [11]. Tin(II) is chelated into an etiopurpurin ($SnET_2$) otherwise known as Purlytin [12]. Indium(III) is present in a chelate of pyropheophorbide methyl ester known as MV6401 [13]. The rare earth metal lutetium(III) is chelated into the tetrapyrrole macrocycle known as texaphyrin to produce motexafin lutetium [14]. Palladium (II) is chelated into two bacteriochlorin compounds, bacteriopheophorbide (TOOKAD or WST-09) [15] and its taurine derivative (WST-11) [16], which have been used for vascular targeting.

In addition to the inherent photophysical characteristics of the chromophore, other important attributes to be considered in the design of potential photosensitizers are the chemical characteristics of the molecule. These characteristics govern uptake by various cell types, and also determine the pharmacokinetics, biodistribution and localization of the photosensitizer at the target site. Recent work has shown that the molecular charge as well as the degree of lipophilicity of the photosensitizers can be important in this regard. Photosensitizers with constitutive cationic charges such as quaternary ammonium groups have been shown to be highly effective antimicrobial photosensitizers compared to molecules that are negatively charged, neutral, or even bear basic amino groups [17,[18]].

In the present report, we have examined the photophysical properties of a set of water-soluble imidazolium-substituted porphyrins that contain central zinc(II), palladium(II), and indium(III) ions. The four porphyrins are shown in Chart 1. Each porphyrin is of the *trans*-AB-type wherein a phenyl group is located at one meso-position, an imidazolium substituent is located at the *trans* meso-position, and the flanking meso-positions lack substituents. Porphyrins **1-Zn** and **2-Zn** are zinc(II) chelates, whereas **2-InCl** contains a chloro-indium(III) chelate, and **2-Pd** is a palladium(II) chelate. The motivation for examining the photophysical properties of this set of compounds is to determine whether these properties correlate with the observed in vitro PDT activity (**2-Pd** > **2-InCl** > **2-Zn** > **1-Zn**; P. Mroz, J. Bhaumik, Z. Aly, H. L. Kee, D. Holten, J. S. Lindsey, M. R. Hamblin, manuscript in preparation). The difference in in vitro PDT activity for the four porphyrins is profound: **2-Pd** is about 4 times better than **2-InCl**, which in turn is about 4 times better than **2-Zn**, which in turn is about 10 times better than **1-Zn**. To better understand the origin of the up to 160-fold difference in reactivity, the photophysical characteristics of the four porphyrins in a variety of media are compared with each other and with hydrophobic porphyrin counterparts in organic solvents. Taken together, the results provide a foundation for evaluating the relative PDT activity of the four porphyrins in terms of the contribution of the central metal ion and the overall charge on the sensitizer.

2. Experimental methods

The synthesis of porphyrins **1-Zn**, **2-Zn**, and **2-Pd** has been reported [19]. The synthesis of **2-InCl** will be described elsewhere. The absorbance and fluorescence spectra, fluorescence yields and excited singlet-state lifetimes of **1-Zn**, **2-Zn**, **2-Pd**, and **2-InCl** were investigated at room temperature in several media: (i) a 3:1 mixture of tetrahydrofuran and methanol (THF/MeOH); (ii) standard aqueous phosphate-buffered saline solution containing 10 mM Na_3PO_4, 137 mM NaCl, 2.7 mM KCl, pH 7.4 (PBS); (iii) the same PBS solution containing 0.1 mg/mL bovine serum albumin (PBS/BSA); (iv) a phosphate-buffered saline solution with

a ten-fold increase in the phosphate concentration, namely 100 mM Na_3PO_4, 137 mM NaCl, 2.7 mM KCl, pH 7.4 (cPBS); and (v) the same cPBS solution containing 0.1 mg/mL bovine serum albumin (cPBS/BSA). To prepare the above aqueous solutions, the porphyrin was first dissolved in a drop of dimethylsulfoxide (DMSO) and diluted using PBS, cPBS, PBS/BSA or cPBS/BSA to the desired porphyrin concentration, with the final volume of DMSO being <1% of the total. Phosphorescence spectral studies on **1-Zn**, **2-Zn**, **2-Pd**, and **2-InCl** porphyrins at 295 K utilized samples in a 3:1 mixture of tetrahydrofuran and methanol (THF/MeOH); studies at 77 K utilized an ethanol glass. Studies on the standard compounds zinc(II)-*meso*-tetraphenylporphyrin (**ZnTPP**) and palladium(II)-*meso*-tetraphenylporphyrin (**PdTPP**) at 295 K utilized toluene, tetrahydrofuran, or pyridine; studies at 77 K used 2-methyltetrahydrofuran (2-MeTHF).

Static absorption (Cary 100) and fluorescence (Spex Fluorolog2) measurements were performed using dilute (μM) solutions. Fluorescence lifetimes were obtained using a phase modulation technique [20]. Argon-purged solutions with an absorbance of ≤0.10 at the Soret-band excitation wavelength were used for the fluorescence spectral and lifetime measurements. Fluorescence spectra were acquired at 0.2 nm data intervals using a band pass for the excitation and detection monochromators of 1.5 and 3.3 nm, respectively, and were corrected for detection-system spectral response. Fluorescence quantum yields were determined using argon-purged solutions and excitation at the peak of the Soret band (405–425 nm) relative to free base *meso*-tetraphenylporphyrin (**FbTPP**) in toluene [$\Phi_f = 0.09$] [21], and its zinc chelate **ZnTPP** in benzene [$\Phi_f = 0.030$] [22]. The fluorescence quantum yields were corrected for solvent refractive index and averaged.

Yields of the lowest excited triplet state (Φ_{isc}) were obtained using argon-purged samples and a transient-absorption technique similar to that described previously [23,[24]]. The extent of bleaching of the ground-state Q(1,0) band at ~500 nm (relative to the featureless transient absorption) due to the lowest singlet excited state was measured immediately following a 130 fs flash in either the Soret (418 nm) or Q (554 to 602 nm) bands. The amplitude of this signal was compared to that due to the lowest triplet excited state, which was derived from two methods. In the first method, the triplet bleaching signal was taken as the long-time asymptote of the fitted exponential singlet-excited-state bleaching decay (4-ns time course) with the time constant fixed at the fluorescence lifetime. In the second method, the triplet bleaching was measured directly at a long (~20 ns) time delay. The triplet yields obtained using the different methods were averaged. For **2-Pd** and **2-InCl**, the excited singlet-state lifetime is sufficiently short so that a delay time of only a few nanoseconds was necessary to accurately determine the triplet-state bleaching using the second method.

The lifetimes of the lowest energy triplet excited state (τ_T) for **1-Zn**, **2-Zn**, and **2-Pd** were measured at room temperature on compounds in ethanol rigorously degassed by the freeze-pump-thaw method (10 cycles each) on a high vacuum system (< 1 micron pressure) and sealed. For some solvents, purging with argon or nitrogen even for >1 h is not sufficient to eliminate the contribution of oxygen quenching. Triplet lifetimes on these three porphyrins were also measured at 77 K in frozen ethanol glasses. Due to its diffusional nature, any residual contribution from quenching by O_2 at room temperature is effectively eliminated in the low-temperature glass. Triplet lifetimes were not measured for **2-InCl** because verifiable phosphorescence was not observed (vide infra). For comparison, triplet decay profiles were also measured for **ZnTPP** and **PdTPP** in 2-MeTHF degassed solutions at room temperature and glasses at 77 K.

Triplet lifetimes were determined using ~7 ns, ~6 mJ, 532 nm excitation flashes from a Q-switched Nd:YAG laser (Quanta Ray DCR-3, Spectra-Physics) and detection with a photodiode (H6780-20, Hamamatsu). The signal was sent to a 50 Ω input of a 1.5 GHz, 20

gigasample/sec digital oscilloscope (TDS7154, Tektronix). The resulting decay traces were fitted to the sum of a Gaussian instrument profile plus a single exponential plus a constant (Igor Pro, Wavemetrics). Alternatively, the lifetimes were obtained by deleting the time points encompassing the instrument profile, and the remainder were fitted to a single exponential plus a constant (Origin, Microcal OriginLab). This method gave the same lifetimes within the reported error limits to that using the full data set, and hence was used for the majority of the analyses.

The room-temperature triplet lifetimes were obtained using excitation flashes that were sufficiently weak to effectively eliminate contributions from triplet-triplet annihilation. This was assessed for **PdTPP** when a further reduction in flash strength did not affect the decay profile or the resulting lifetime obtained from a single-exponential fit. Similarly **2-Pd** did not change with a >10-fold reduction in flash intensity from the level used to obtain the reported lifetimes. Additionally, due to the diffusional nature of triplet-triplet annihilation, any residual contribution from these processes at room temperature is effectively eliminated in the low-temperature glass.

The molar absorption (extinction) coefficients (ε) for **ZnTPP**, **ZnOEP**, and **PdOEP** (OEP is 2,3,7,8,12,13,17,18-octaethylporphyrin) in toluene were determined by dissolving a measured amount in 25 mL of toluene. The stock solution was then diluted 20x for absorption measurement. The value of ε was calculated for three trials and averaged from the absorbance at the peak of the Soret band. The values (vide infra) agree with those in the literature [25–27].

3. Results and discussion

3.1. Absorption spectra in organic solvents

The electronic ground-state absorption spectra of the four metalloporphyrins **1-Zn**, **2-Zn**, **2-Pd**, and **2-InCl** (Chart 1) in THF/MeOH solution at room temperature are shown in Fig. 1 (solid lines). The spectrum of each compound shows a strong near-UV Soret (B) band (corresponding to $S_0 \rightarrow S_2$) and a pair of weaker visible Q(1,0) and Q(0,0) bands (corresponding to $S_0 \rightarrow S_1$). The peak wavelengths and intensity ratios are listed in Table 1. Several differences in principle could influence relative PDT activity. The full-width-at-half-maximum (FWHM) of the Soret band increases in the order **1-Zn** (11 nm) ~ **2-Zn** (12 nm) < **2-Pd** (24 nm) < **2-InCl** (38 nm) in THF/MeOH. The Q(0,0)/Q(1,0) ratio increases in the order **1-Zn** (0.4) < **2-Zn** (0.7) < **2-Pd** (1.0) < **2-InCl** (2.3). The Soret and Q features of palladium porphyrin **2-Pd** are generally blue shifted from those of the two zinc porphyrins (**1-Zn** and **2-Zn**), whereas those for chloro-indium porphyrin (**2-InCl**) are red shifted.

The modest differences in the absorption characteristics of **1-Zn** versus **2-Zn** must arise from another type of interaction because the sulfonate groups of **1-Zn** are not conjugated to the macrocycle. In this regard, the four-carbon alkyl linkages between the imidazolium and sulfonate groups of **1-Zn** permit the latter group to extend above the plane of the macrocycle. This would place a negative charge in close proximity to the π-electron cloud of the porphyrin and perturb the molecular-orbital energies and thus the optical spectra [28]. Additionally, the alkyl linkages may be sufficiently long to allow a sulfonate oxygen to coordinate to the central zinc ion of the same (or another) porphyrin. Interactions of this type are not possible for the other three metalloporphyrins (Chart 1).

The spectral differences between **2-Pd** and **2-Zn** or **1-Zn** are generally similar to those observed for other types of palladium versus zinc porphyrins. The Soret FWHM is greater for **PdTPP** (17 nm) than **ZnTPP** (12 nm) in toluene, and this is accompanied by a decreased peak extinction coefficient. The latter point is illustrated by the following comparisons of values determined

here or previously (units $M^{-1}cm^{-1}$): **PdTPP** (417 nm) (202 000 [25]) versus **ZnTPP** (423 nm) (571 000; 574 000 [26]) and **PdOEP** (392 nm) (231 000; 191 000 [27]) versus **ZnOEP** (403 nm) (403 000; 417 000 [26]).

The increased breadth of the spectral features of **2-InCl** (Fig. 1D) compared to the other porphyrins may reflect the presence of multiple species that differ in the solvent coordination to the central metal ion. Plausibly, the solvent may also displace the chloride counterion, thereby affecting the position of the metal with respect to the mean macrocycle plane and thus the absorption spectrum.

The shifts in the Q band-positions reflect differences in the energy of the porphyrin S_1 excited state in the order Pd(II) > Zn(II) > In(III)Cl (Table 1). The change in the Q(0,0)/Q(1,0) intensity ratio with metal ion undoubtedly reflects changes in the relative energies of the frontier molecular orbitals and thus the overall oscillator strength of the $S_0 \rightarrow S_1$ absorption contour [29].

A potential contributor to PDT activity is the difference among the metalloporphyrins in the propensity to bind axial ligands to the central metal ion. In order to assess this difference for the imidazolium-substituted palladium (**2-Pd**) and zinc (**1-Zn**, **2-Zn**) porphyrins, spectra were acquired for the reference compounds (**ZnTPP** and **PdTPP**) in several organic solvents that differ in metal-coordination strength (Fig. 2). Axial ligation to a metalloporphyrin generally results in shifts of all the absorption features and a change in the intensity of the Q(0,0) band with respect to the Q(1,0) band. For example, axial ligation of **ZnTPP** red shifts the absorption features and increases the Q(0,0)/Q(1,0) intensity ratio. Figure 2A demonstrates the well known behavior that the central zinc ion of **ZnTPP** is coordinated strongly by pyridine and to a lesser degree by THF; coordination by toluene does not occur. On the other hand, the Q band ratio is not perturbed for **PdTPP** even in pyridine (Fig. 2B). The solvent only marginally shifts the Soret feature, which can be attributed to solvent polarity rather than axial ligation. Thus, the zinc porphyrins (e.g., **2-Zn**) have a much greater propensity for axial ligation than palladium porphyrins (e.g., **2-Pd**).

3.2. Absorption spectra in aqueous media

Absorption spectra were acquired for the porphyrins in aqueous PBS and in the presence of bovine serum albumin (PBS/BSA) to explore some of the types of interactions that may be present in the biological milieu (Fig. 3). The differences from the spectra in THF/MeOH are largest in the Soret region, with relatively small perturbations to the Q bands (Table 1). Figure 3B shows that **2-Zn** has an additional component on the long wavelength side of the Soret feature in PBS that collapses upon the addition of BSA (except for a small band shift from the position in THF/MeOH). These observations can be explained by aggregates of positively charged **2-Zn** formed in PBS being disrupted by the binding to the overall negatively charged BSA protein [30], which also shifts the band due to a dielectric effect.

Similar behavior is observed for **1-Zn** (Fig. 3A), although the effect of BSA is less pronounced than for **2-Zn** because in this case the porphyrin (like BSA) bears an overall negative charge. Aggregation of **2-Pd** in PBS is also disrupted by BSA (Fig. 3C); residual aggregation or a greater heterogeneity of porphyrin-medium interactions can explain the increased spectral width in aqueous versus THF/MeOH solutions. The presence of aggregation and effects of BSA are less apparent for **2-InCl** (Fig. 3D).

3.3. Emission spectra

Emission spectra for the four porphyrins in deoxygenated THF/MeOH solutions at room temperature are shown in Fig. 1 (dashed lines). For zinc porphyrins **1-Zn** and **2-Zn**, the

emission spectra are dominated by $S_1 \rightarrow S_0$ fluorescence (Figs. 1A and 1B). For both compounds, the shorter-wavelength feature is the Q(0,0) band and the longer-wavelength feature is the Q(0,1) vibronic satellite. The Q(0,0) fluorescence peak is shifted by ~5 nm (~180 cm^{-1}) from the corresponding absorption maximum (Table 1). The difference in the intensity ratio of the two fluorescence bands for **1-Zn** and **2-Zn** qualitatively parallels that observed for the absorption bands.

The emission spectrum for **2-InCl** is also dominated by $S_1 \rightarrow S_0$ fluorescence (Fig. 1D). The nominal Q(0,0) fluorescence feature for this compound has several underlying components that parallel those seen in the Q(0,0) absorption profile; whatever the molecular origin (e.g., axial-ligation states, macrocycle conformation), the different molecular components are clearly emissive. The emission spectrum of **2-Pd** is much different from the other three compounds (Fig. 1C). The Q(0,0) and Q(0,1) fluorescence features for this compound are quite weak and are barely observed at the expected positions with respect to the origin absorption band in deoxygenated solution. Instead, the emission spectrum is dominated by $T_1 \rightarrow S_0$ phosphorescence bands, T(0,0) and T(0,1), that lie at substantially longer wavelengths (Table 1). Upon introduction of oxygen into the sample, the phosphorescence is dramatically quenched, so that only fluorescence is observed. The emission spectrum for **2-Pd** in oxygenated THF/MeOH solution is shown in Fig. 1C (dotted line).

The relative intensities of the fluorescence and phosphorescence emission for the porphyrins were examined further in ethanol glasses at 77 K (Fig. 4). The frozen medium results in sharper bands than in fluid solution at room temperature and eliminates diffusion-controlled quenching of the (phosphorescence) triplet excited state by any residual trace O_2 and by triplet-triplet encounters. Each spectrum in Fig. 4 is normalized to the peak intensity of the strongest emission band, which is the Q(1,0) fluorescence peak for **1-Zn** and **2-Zn** and the T(0,0) phosphorescence feature for **2-Pd**. Although fluorescence was observed for **2-InCl** at 77 K (Table 1), phosphorescence could not be verified by excitation spectra; thus, a low-temperature emission spectrum for this complex is not shown.

The low-temperature emission spectra for the two zinc porphyrins are basically identical to one another (Figs. 4A and 4B) with the following characteristics: Q(0,0), 579 nm; Q(0,1), 633 nm; Q(2,0), 685 nm; T(0,0), 738 nm; T(0,1), 823 nm. The T(0,0) position places the lowest triplet excited state (T_1) at 1.68 eV above the S_0 ground state, and the spacing from the Q(0,0) band places the T_1 state 0.46 eV (3710 cm^{-1}) below the S_1 excited state (Table 2). These values are comparable to those found here (Table 2) and previously [29] for **ZnTPP**. The ratio of the integrated phosphorescence profile [encompassing T(0,0) and T(0,1)] and the fluorescence profile [encompassing Q(0,0), Q(0,1) and Q(0,2)] gives the ratio of the phosphorescence to fluorescence quantum yields (Φ_p/Φ_f). This quantum-yield ratio is 0.11 for **1-Zn** and 0.14 for **2-Zn** at 77 K, which are comparable to the ratio of 0.11 for **ZnTPP** (Table 2).

The low-temperature emission spectrum for **2-Pd** (Fig. 4C), like that at room temperature (Fig. 1C), exhibits strong phosphorescence but only very weak fluorescence. The features are Q (0,0), 542 nm; Q(0,1), 590 nm; Q(2,0), 620 nm; T(0,0), 657 nm; T(0,1), 732 nm. The T(0,0) position places the T_1 excited state at 1.89 eV about the ground state, which is 0.21 eV higher than for the two zinc porphyrins. The Q(0,0) – T(0,0) spacing for **2-Pd** corresponds to a singlet-triplet splitting of 0.40 eV (3226 cm^{-1}), which is comparable to that for **PdTPP** and only marginally smaller than that for **1-Zn**, **2-Zn** and **ZnTPP** (Table 2). The value of Φ_p/Φ_f is 650 for **2-Pd**, which is comparable to $\Phi_p/\Phi_f > 460$ for **PdTPP** and roughly 5000-fold greater than the values for **1-Zn** and **2-Zn**.

Fluorescence for **2-InCl** is also observed in a 77-K ethanol glass (Table 1) and has similar characteristics to the room-temperature spectrum in THF/MeOH solution (Fig. 1D). The

singlet-triplet splittings observed for the zinc and palladium porphyrins, together with the significantly red-shifted position of the Q(0,0) band for **2-InCl** (Fig. 1D), predict that the T (0,0) phosphorescence for the latter complex should be found near 820 nm (~1.5 eV above the ground state). Although weak emission features were observed between 750 nm and 870 nm for **2-InCl** at 77 K, they could not be unambiguous assigned to the parent complex by excitation spectroscopy.

3.4. Singlet excited-state lifetimes, fluorescence yields, and triplet yields

The lifetime of the lowest singlet excited state (τ_S), the fluorescence quantum yield (Φ_f), and the yield of intersystem crossing to the lowest triplet excited state (Φ_{isc}) for each of the four porphyrins in THF/MeOH at 295 K are given in Table 2. The fluorescence yields for zinc porphyrins **1-Zn** and **2-Zn** (~0.015) are two-fold smaller than for **ZnTPP** (0.03) whereas the excited-state lifetimes are about 30% longer (3.0 ns versus 2.1 ns) [22,[31]]. The close similarities in properties of **1-Zn** and **2-Zn** indicate that the net charge on the meso substituent has little impact (Chart 2). Furthermore, the differences from reference porphyrin **ZnTPP** are modest and must simply be due to the presence of two versus four meso aryl substituents. In addition, for both **1-Zn** and **2-Zn**, the τ_S and Φ_f values are similar in aqueous solution to those found in THF/MeOH, and there is little effect upon the addition of BSA (Table 1).

Compared to the zinc porphyrins, chloro-indium porphyrin **2-InCl** is less fluorescent (Φ_f ~0.008) and has a 13-fold shorter singlet excited-state lifetime (240 ps). These values are comparable to the quantum yields and lifetimes for dichloro-tin(IV) porphyrins, which the S_1 and T_1 states are also expected to be (π,π^*) in nature because the metal has a closed 3d-shell [23,[32]].

The differences in excited-state properties are even more prominent for **2-Pd**, which is barely fluorescent ($\Phi_f = 1.2 \times 10^{-4}$) and has a singlet excited-state lifetime (9 ps) that is about 300-fold shorter than those for **2-Zn** and **1-Zn**. The fluorescence quantum yield for **2-Pd** is comparable to that for **PdTPP** [25,[29]]. This Φ_f combined with an average natural radiative rate constant of $k_f \sim (60\ ns)^{-1}$ for metallotetraphenylporphyrins [22,[29]] predicts $\tau_S = \Phi_f/k_f = \Phi_f \cdot (60\ ns)^{-1} \sim 10$ ps for **PdTPP**, in good agreement with the value measured here for **2-Pd**.

The measured intersystem-crossing yields (Table 2) increase in the order: **2-Pd** (0.88) > **2-InCl** (0.83) > **2-Zn** and **1-Zn** (0.79 and 0.69). Given that the uncertainty (± 10%) in these values somewhat obscures the true impact of the metal ion on the intersystem-crossing process, an additional estimate for Φ_{isc} for each compound is derived below.

3.5. Decay properties of the lowest-energy singlet excited state

The observables τ_S, Φ_f, and Φ_{isc} for decay of the lowest-energy singlet excited state are connected to the rate constants for $S_1 \rightarrow S_0$ spontaneous fluorescence (k_f), $S_1 \rightarrow S_0$ internal conversion (k_{ic}), and $S_1 \rightarrow T_1$ intersystem crossing (k_{isc}) via Eqs. (1) to (3).

$$\tau_s = (k_f + k_{ic} + k_{isc})^{-1} \quad (1)$$

$$\Phi_f = k_f/(k_f + k_{ic} + k_{isc}) \quad (2)$$

$$\Phi_{isc} = k_{isc}/(k_f + k_{ic} + k_{isc}) \quad (3)$$

The radiative rate constant can be calculated from the observables via Eq. (4).

$$k_f = \Phi_f / \tau_s \quad (4)$$

Similarly the intersystem-crossing rate constant can be calculated via Eq. (5).

$$k_{isc} = \Phi_{isc} / \tau_s \quad (5)$$

A second estimate for the intersystem crossing rate constant is obtained via Eq. (6).

$$k_{isc}^{ref} = (\tau_s)^{-1} - k_f - k_{ic} \quad (6)$$

The "ref" denotation indicates that the calculation in Eq. (6) for **1-Zn**, **2-Zn**, **2-Pd**, and **2-InCl** utilizes a common value of k_{ic} = (16.2 ns)$^{-1}$ derived for **ZnTPP** (using Eqs. (1) to (4) and the associated τ_S, Φ_f, and Φ_{isc} values). The assumption of a (relatively) constant $S_1 \rightarrow S_0$ internal-conversion rate constant (k_{ic}) among the related meso-substituted metalloporphyrins is reasonable because the molecules have similar structural characteristics and a comparable singlet energy gap from the ground state. Subsequently, the value of k_{isc}^{ref} obtained from Eq. (6) for each compound was used to obtain an additional estimate for the intersystem-crossing yield via Eq. (7).

$$\Phi_{isc}^{ref} = k_{isc}^{ref} \bullet \tau \quad (7)$$

The rate constant and yield obtained using Eqs. (1) to (7) for each metalloporphyrin are given in Table 2. The radiative rate constant (k_f) varies with the central metal ion as follows: **1-Zn** [Zn(II), (214 ns)$^{-1}$] ~ **2-Zn** [Zn(II), (200 ns)$^{-1}$] < **2-Pd** [Pd(II), (75 ns)$^{-1}$] < **2-InCl** [Cl-In(III), (31 ns)$^{-1}$]. This trend tracks the Q-absorption oscillator strength as exemplified by the Q(0,0)/Q(1,0) intensity ratio (Fig. 1, Table 1): **1-Zn** (0.4) < **2-Zn** (0.7) < **2-Pd** (1.0) < **2-InCl** (2.3). The Q(0,0)/Q(1,0) tracks the $S_1 \rightarrow S_0$ oscillator strength because the Q(1,0) intensity is derived from vibronic borrowing from the Soret transition and is thus relatively constant [29,[33]]. In turn, the $S_0 \rightarrow S_1$ (stimulated) absorption oscillator strength is proportional to k_f for $S_1 \rightarrow S_0$ (spontaneous) fluorescence via the Einstein coefficients.

As noted above, the four metalloporphyrins exhibit modest differences in the measured yields of $S_1 \rightarrow T_1$ intersystem crossing (Φ_{isc}): **2-Pd** (0.88) > **2-InCl** (0.83) > **2-Zn** (0.79) > **1-Zn** (0.69). These values together with the S_1 lifetime (τ_S) and Eq. (5) give the intersystem-crossing rate constants (k_{isc}): **2-Pd** [(10 ps)$^{-1}$] > **2-InCl** [(290 ps)$^{-1}$] > **2-Zn** [(3.8 ns)$^{-1}$] > **1-Zn** [(4.3 ns)$^{-1}$]. Although the k_{isc} values exhibit the same trend as Φ_{isc}, the spread is much greater and better indicates differences among the complexes. Nonetheless, the uncertainties in the Φ_{isc} determinations transform into uncertainties in the k_{isc} values. Thus, the effect of the metal ion on the intersystem-crossing process is better reflected in the k_{isc}^{ref} and Φ_{isc}^{ref} values, which follow the trend **2-Pd** [Pd(II), (9 ps)$^{-1}$, >0.99] > **2-InCl** [Cl-In(III), (250 ps)$^{-1}$, 0.98] > **1-Zn** [Zn(II), (3.7 ns)$^{-1}$, 0.8] ~ **2-Zn** [Zn(II), (3.8 ns)$^{-1}$, 0.8]. The values necessarily track the measured singlet excited-state decay rate (i.e., the inverse of the observed lifetime τ_S): 2-Pd (9 ps)$^{-1}$ > **2-InCl** (240 ps)$^{-1}$ > **1-Zn** (3 ns)$^{-1}$ ~ **2-Zn** (3 ns)$^{-1}$.

The large differences between **2-Pd** versus **1-Zn** and **2-Zn** are expected due to the heavy-atom effect on the spin-orbit coupling that drives the $S_1 \rightarrow T_1$ conversion [29,[34]]. Due to similar atomic numbers, In(III) might be expected to have a comparable spin-orbit effect as Pd(II); however the latter may be more effective due to stronger interactions with the porphyrin core-nitrogen atoms via d-orbital participation in π-backbonding.

3.6. Decay properties of the lowest energy triplet excited state

The T_1 decay profiles in frozen glasses at 77 K are single exponential (no significant O_2-quenching or triplet-triplet annihilation effects) with time constants (τ_T) that reflect the intrinsic decay processes ($T_1 \rightarrow S_0$ phosphorescence and $T_1 \rightarrow S_0$ intersystem crossing). The τ_T values for the two zinc porphyrins **1-Zn** and **2-Zn** at 77 K are 64 ms and 54 ms, respectively. These lifetimes are about two-fold longer than the lifetimes obtained here (Table 2) and previously [29,[34]] for **ZnTPP**. The value τ_T = 2.0 ms for **2-Pd** is comparable to the values found here (Table 2) and previously [34,[35]] for **PdTPP**. For each compound, the value of τ_T is input into Eq. (8) to obtain a value for the phosphorescence rate constant k_p using the values for the yields of intersystem-crossing (Φ_{isc}^{ref}) and phosphorescence (Φ_p) given in Table 2.

$$k_p = \frac{\Phi_p}{\Phi_{isc}^{ref} \bullet \tau_T} \tag{8}$$

The resulting k_p value for **2-Pd** [$(26\ ms)^{-1}$] is 1000-fold greater than for **2-Zn** and **1-Zn** [$(21\ s)^{-1}$ and $(33\ s)^{-1}$], consistent with heavy-atom enhancement of spin-orbit coupling.

3.7. Triplet decay at room temperature and quenching by molecular oxygen

The τ_T values for **2-Zn**, **1-Zn** and **ZnTPP** in fluid solution at 295 K (6.1, 4.5, 4.6 ms) are considerably shorter than those found in the frozen medium at 77 K (33, 54, 64 ms). The triplet lifetime for **PdTPP** at room temperature (110 μs) is again about 50-fold shorter than for the zinc porphyrins, like that at low temperature (1.5 ms). Surprisingly, the τ_T value for **2-Pd** at 295 K is 10-fold shorter (10 μs) than that for **PdTPP** even though they have essentially the same lifetime at 77 K (2.0 ms). The lifetime for **2-Pd** is identical (10 μs) in degassed ethanol and 2-MeTHF, so the difference from **PdTPP** in 2-MeTHF is not due to a solvent effect. The shorter τ_T for **2-Pd** cannot be ascribed to residual triplet-triplet annihilation because the decay is single exponential and remains at 10 μs even with a 10-fold reduction in flash strength (where annihilation did not contribute for **PdTPP**). Thus, the short room-temperature τ_T for **2-Pd** is unexplained.

Although the triplet lifetimes for **2-Pd** and **PdTPP** in degassed solution at room temperature differ by an order of magnitude, the lifetime for both compounds in air-saturated 2-MeTHF (and in ethanol for **2-Pd**) is the same (300 ns). This value is comparable to the lifetime obtained previously for **PdTPP** in air-saturated toluene [25]. Because this lifetime is substantially shorter than those obtained for both palladium porphyrins in degassed solution, and assuming minimal or no triplet-triplet annihilation, the decay kinetics are dominated by the term $k_q[O_2]$. Assuming an O_2 concentration of 2 mM in the air-saturated organic solvent [36,[37]], a lifetime of 300 ns corresponds to a quenching rate constant of $k_q = 1.7 \times 10^9\ M^{-1}s^{-1}$. Analogous studies on zinc porphyrins **2-Zn**, **1-Zn** and **ZnTPP** in air-saturated 2-MeTHF give triplet lifetimes of ~100 ns and $k_q \sim 5 \times 10^9\ M^{-1}s^{-1}$; the errors in the latter determinations are larger than those for the palladium porphyrins due to the significantly reduced phosphorescence intensities.

The k_q values obtained above are comparable to the rate constants obtained for O_2 quenching of the triplet excited states of a variety of porphyrins [38] and inorganic complexes [39]. The values are about one-ninth of the (diffusion-limited) rate of O_2 quenching by singlet excited states, with the reduction factor being ascribed to spin restrictions for triplet-triplet energy transfer to produce two singlet states (excited O_2 and ground-state porphyrin) [40–42]. On the basis of prior analyses of oxygen quenching of excited chromophores [37], the observed lifetimes and derived quenching rate constant imply that essentially every (>90%) triplet state produced for these porphyrins in air-saturated solution is quenched by reaction with O_2.

3.8. Implications of the photophysical properties for relative PDT activity

As noted in the Introduction, the in vitro PDT activity differs for the four porphyrins: **2-Pd** is about 4 times better than **2-InCl**, which in turn is about 4 times better than **2-Zn**, which in turn is about 10 times better than **1-Zn**. The PDT activity was assayed in murine CT26 colon adenocarcinoma and human HeLa cervical carcinoma cells. Differences between the compounds for cell uptake and related assays were performed. A detailed discussion of these measurements, results, and the mechanism(s) of PDT activity will be presented elsewhere (P. Mroz, J. Bhaumik, Z. Aly, H. L. Kee, D. Holten, J. S. Lindsey, M. R. Hamblin, manuscript in preparation). The following provides a foundation for understanding the extent to which the photophysical properties investigated herein contribute to the observed differences in PDT activity.

Given that the photophysical behavior of the two zinc porphyrins (**2-Zn** and **1-Zn**) are identical except for small differences in spectral characteristics, the observed 10-fold differences in PDT activity of these two compounds must derive from the two (negatively charged) sulfonate-terminated alkyl groups attached to the imidazolium substituent of **1-Zn** (Chart 1). As can be seen from Fig. 2, these two molecules clearly differ in their potential interactions with proteins (e.g., BSA). In this regard, there is evidence that cationic PDT agents better localize than anionic analogues in certain types of cells [17,18].

The remaining discussion focuses on the homologous set of porphyrins (**2-Pd**, **2-Zn**, **2-InCl**) bearing the same meso-substituents (phenyl and imidazolium). For the broad-band illumination (400–700 nm; 10 J/cm^2) used in the in vitro PDT experiments, the (comparable) absorption properties of the compounds should not play a dominant role in dictating the relative PDT activities. Although the trend in $S_1 \rightarrow T_1$ intersystem-crossing yields [**2-Pd** (>0.99), **2-Zn** (0.8)] tracks the observed PDT activity, this contributes only a factor of ~1.3, which is much smaller than the observed 16-fold effect. Furthermore, if the porphyrin series were extended to include a free base analogue (e.g., $\Phi_{isc} \sim 0.76$ for **FbTPP** [21,43–46]), then a maximal enhancement of only a factor of ~1.4 in PDT efficacy would be predicted across a series that ranges from metal-free to heavy-metal (e.g., palladium) porphyrins.

The enhanced spin-orbit coupling that underlies the greater $S_1 \rightarrow T_1$ yields (Φ_{isc}) also underlies the 1000-fold greater $T_1 \rightarrow S_0$ radiative rate (k_p) for **2-Pd** versus **2-Zn** (Table 2). The impact would be significant if even a fraction of this factor contributes to the relative probabilities for energy (or electron) transfer from the T_1 excited state of the porphyrin to $^3O_2$. The associated increased mixing of the T_1 and S_0 states should help drive the porphyrin from T_1 to S_0 and enhance energy transfer to $^3O_2$. In principle, this could involve dipole-dipole coupling, electron-exchange interactions, or relaxation of spin restrictions. These effects are generally not realized, at least in the air-saturated solutions, because for a range of porphyrins the quantum yield of T_1 quenching by $^3O_2$ is generally the same as the T_1 yield [25,38].

On the other hand, it is possible that the situation is different in some biological milieu. The O_2 concentration may be sufficiently low that during the T_1 lifetime only a small fraction will encounter an O_2 molecule and/or that each collision is not effective in producing energy/

electron transfer. In this case, enhanced T_1–S_0 coupling for **2-Pd** versus **2-Zn** would complement the small (1.3-fold) difference in triplet yields and play a role in the 16-fold greater PDT efficacy of the former versus the latter sensitizer.

For most sensitizers, energy transfer from the T_1 excited state of the sensitizer to $^3O_2$ to produce the reactive $^1O_2$ excited-singlet species is thought to play a role in PDT activity (Type-II mechanism). For some sensitizers and some cellular environments, PDT efficacy is thought to be enhanced by photo-oxidation of the sensitizer via electron transfer from T_1 to $^3O_2$ and subsequent processes to give reactive species such as superoxide or hydroxyl radicals, even if produced in low yield (Type-I mechanism). The potential roles of these various reactive oxygen species produced by the palladium bacteriochlorin sensitizer TOOKAD in different environments have been described [15,[47]]. If the rate and efficiency of the T_1 photo-oxidation step in the Type-I mechanism is the limiting factor, then the PDT efficacy should track the excited-state oxidation potential of the sensitizer.

With regard to **2-Pd** and **2-Zn**, the excited-state oxidation potentials of these two sensitizers are comparable. This conclusion follows because palladium porphyrins are harder to oxidize than zinc porphyrins by 0.2 to 0.3 V in the ground state [48], which is counterbalanced by the T_1 excited-state energies of the former being above those of the latter by ~0.2 eV (Table 2). On the other hand, palladium porphyrins are easier to reduce than zinc porphyrins by ~0.2 V in the ground state [48], which complements the T_1 energy difference to make the excited state of **2-Pd** a more potent electron acceptor than **2-Zn** by ~0.4 V. Thus if operable in the cellular environment, a two-step mechanism involving an exogenous electron donor and intermediate photoreduction of the porphyrin T_1 state prior to electron transfer to $^3O_2$ could complement the modestly higher intersystem-crossing yield in enhancing the PDT activity of **2-Pd** versus the other sensitizers.

These considerations suggest that if the standard Type-II electron-transfer mechanism (sensitizer T_1 photo-oxidation) plays a role in the difference in PDT activity of the **2-Pd** versus **2-Zn**, then other factors involved in the ultimate formation of the reactive radical species must come into play. One could be differences in the cellular sites of localization of the two sensitizers, which would also contribute to the relative PDT efficacies of the two compounds by the Type-II mechanism. The importance of the immediate environment of a sensitizer in the relative yields of various reactive oxygen species (produced by energy or electron transfer) has been discussed in the context of studies of the palladium bacteriochlorin TOOKAD [15, [47]]. Given that **2-Pd**, **2-InCl, and 2-Zn** have the same peripheral groups, attention must be focused on the ligation properties of the central metal ion. Palladium porphyrins do not acquire axial ligands with near the propensity as zinc porphyrins (**2-Pd** and **2-Zn**; Fig. 2). Indium porphyrins bind a negatively charged apical ligand. Thus, **2-Pd** will not ligate entities from the medium or biological milieu to near the extent as **2-Zn**, **1-Zn**, or **2-InCl**. Thus, the smaller hydrodynamic radius of the palladium porphyrin (compared to porphyrins with axial ligands), and reduced propensity for metal-derived interactions, may enable greater delivery of **2-Pd** to the target site, or perhaps the precise binding site itself. Such differences could be intertwined with the production of the ultimate reactive oxygen species. Collectively, the studies reported here provide a framework for understanding the factors that underlie the differences in observed PDT activity of the imidazole-substituted (charged) zinc, palladium, and indium porphyrins.

Acknowledgments

This work was supported by grants from the National Institutes of Health (GM36238 to JSL and AI050875 to MRH). HLK was supported by the Imaging Sciences Pathway training grant from the NIH (5T90 DA022871) at Washington University.

References

1. Agostinis P, Buytaert E, Breyssens H, Hendrickx N. Regulatory pathways in photodynamic therapy induced apoptosis. Photochem Photobiol Sci 2004;3:721–729. [PubMed: 15295626]
2. Hamblin MR, Hasan T. Photodynamic therapy: a new antimicrobial approach to infectious disease? Photochem Photobiol Sci 2004;3:436–350. [PubMed: 15122361]
3. Dolmans DE, Fukumura D, Jain RK. Photodynamic therapy for cancer. Nat Rev Cancer 2003;3:380–387. [PubMed: 12724736]
4. Krammer B. Vascular effects of photodynamic therapy. Anticancer Res 2001;21:4271–4277. [PubMed: 11908681]
5. Rockson SG, Lorenz DP, Cheong WF, Woodburn KW. Photoangioplasty: an emerging clinical cardiovascular role for photodynamic therapy. Circulation 2000;102:591–596. [PubMed: 10920074]
6. Castano AP, Demidova TN, Hamblin MR. Mechanisms in photodynamic therapy: part one–photosensitizers, photochemistry and cellular localization. Photodiag Photodyn Ther 2004;1:279–293.
7. Foote CS. Definition of type I and type II photosensitized oxidation. Photochem Photobiol 1991;54:659. [PubMed: 1798741]
8. Nyman ES, Hynninen PH. Research advances in the use of tetrapyrrolic photosensitizers for photodynamic therapy. J Photochem Photobiol B 2004;73:1–28. [PubMed: 14732247]
9. Rodal GH, Rodal SK, Moan J, Berg K. Liposome-bound Zn(II)-phthalocyanine. Mechanisms for cellular uptake and photosensitization. J Photochem Photobiol B 1998;45:150–159. [PubMed: 9868805]
10. Stern SJ, Craig JR, Flock S, Small S. Effect of aspirin on photodynamic therapy utilizing chloroaluminum sulfonated phthalocyanine (CASP). Lasers Surg Med 1992;12:494–499. [PubMed: 1406001]
11. Egorin MJ, Zuhowski EG, Sentz DL, Dobson JM, Callery PS, Eiseman JL. Plasma pharmacokinetics and tissue distribution in CD2F1 mice of Pc4 (NSC 676418), a silicone phthalocyanine photodynamic sensitizing agent. Cancer Chemother Pharmacol 1999;44:283–294. [PubMed: 10447575]
12. Mang TS, Allison R, Hewson G, Snider W, Moskowitz R. A phase II/III clinical study of tin ethyl etiopurpurin (Purlytin)-induced photodynamic therapy for the treatment of recurrent cutaneous metastatic breast cancer. Cancer J Sci Am 1998;4:378–384. [PubMed: 9853137]
13. Ciulla TA, Criswell MH, Snyder WJ, Small W IV. Photodynamic therapy with PhotoPoint photosensitiser MV6401, indium chloride methyl pyropheophorbide, achieves selective closure of rat corneal neovascularisation and rabbit choriocapillaris. Br J Ophthalmol 2005;89:113–119. [PubMed: 15615758]
14. Yeung PF. Motexafin lutetium (Pharmacyclics). Inv Drugs 2001;4:351–359.
15. Vakrat-Haglili Y, Weiner L, Brumfeld V, Brandis A, Salomon Y, McIlroy B, Wilson BC, Pawlak A, Rozanowska M, Sarna T, Scherz A. The microenvironment effect on the generation of reactive oxygen species by Pd-bacteriopheophorbide. J Am Chem Soc 2005;127:6487–6497. [PubMed: 15853357]
16. Mazor O, Brandis A, Plaks V, Neumark E, Rosenbach-Belkin V, Salomon Y, Scherz A. WST11, A novel water-soluble bacteriochlorophyll derivative; cellular uptake, pharmacokinetics, biodistribution and vascular-targeted photodynamic activity using melanoma tumors as a model. Photochem Photobiol 2005;81:342–351. [PubMed: 15623318]
17. Caminos DA, Spesia MB, Durantini EN. Photodynamic inactivation of Escherichia coli by novel meso-substituted porphyrins by 4-(3-N,N,N-trimethylammoniumpropoxy)phenyl and 4-(trifluoromethyl)phenyl groups. Photochem Photobiol Sci 2006;5:56–65. [PubMed: 16395428]
18. Milanesio ME, Alvarez MG, Silber JJ, Rivarola V, Durantini EN. Photodynamic activity of monocationic and non-charged methoxyphenylporphyrin derivatives in homogeneous and biological media. Photochem Photobiol Sci 2003;2:926–933. [PubMed: 14560810]
19. Bhaumik J, Yao Z, Borbas KE, Taniguchi M, Lindsey JS. Masked imidazolyl-dipyrromethanes in the synthesis of imidazole-substituted porphyrins. J Org Chem 2006;71:8807–8817. [PubMed: 17081010]

20. Kee HL, Kirmaier C, Yu L, Thamyongkit P, Youngblood WJ, Calder ME, Ramos L, Noll BC, Bocian DF, Scheidt WR, Birge RR, Lindsey JS, Holten D. Structural control of the photodynamics of boron-dipyrrin complexes. J Phys Chem B 2005;43:20433–20443. [PubMed: 16853644]
21. Gradyushko AT, Sevchenko AN, Solovyov KN, Tsvirko MP. Energetics of photophysical processes in chlorophyll-like molecules. Photochem Photobiol 1970;11:387–400. [PubMed: 5456267]
22. Seybold PG, Gouterman M. Porphyrins XIII. Fluorescence spectra and quantum yields. J Mol Spectrosc 1969;31:1–13.
23. Magde D, Windsor MW, Holten D, Gouterman M. Picosecond flash photolysis: transient absorption in Sn(IV), Pd(II), and Cu(II) porphyrins. Chem Phys Lett 1974;29:183–188.
24. Tait CD, Holten D. Effects of Mg-solvent coordination state on some excited state processes of bacteriochlorophyll a. Photobiochem Photobiophys 1983;6:201–209.
25. Wiehe A, Stollberg H, Runge S, Paul A, Senge MO, Roder B. PDT-related photophysical properties of conformationally distorted palladium(II) porphyrins. J Porphyrins Phthalocyanines 2001;5:853–860.
26. Dixon JM, Taniguchi M, Lindsey S. PhotochemCAD 2. A refined program with accompanying spectral databases for photochemical calculations. Photochem Photobiol 2005;81:212–213. [PubMed: 15571431]
27. Smith, KE. Porphyrins and Metalloporphyrins. Elsevier Scientific; New York: 1975. p. 885
28. Hanson LK, Fajer J, Thompson MA, Zerner MC. Electrochromic effects of charge separation in bacterial photosynthesis: theoretical models. J Am Chem Soc 1987;109:4728–4730.
29. Gouterman, M. The Porphyrins. Dolphin, D., editor. Vol. III. Academic Press; New York: 1978. p. 1-165.
30. Tribet C, Porcar I, Bonnefont PA, Audebert R. Association between hydrophobically modified polyanions and negatively charged bovine serum albumin. J Phys Chem B 1998;102:1327–1333.
31. Tomizaki K, Loewe RS, Kirmaier C, Schwartz JK, Retsek JL, Bocian DF, Holten D, Lindsey JS. Synthesis and photophysical properties of light-harvesting arrays comprised of a porphyrin bearing multiple perylene-monoimide accessory pigments. J Org Chem 2002;67:6519–6534. [PubMed: 12201776]
32. Gouterman M, Schwarz FP, Smith PD, Dolphin D. Porphyrins. XXVII. Spin-orbit coupling and luminescence of Group IV complexes. J Chem Phys 1973;59:676–690.
33. Perrin MH, Gouterman M. Vibronic coupling. IV. Trimers and trigonal molecules. J Chem Phys 1967;46:1019–1028.
34. Harriman A. Luminescence of porphyrins and metalloporphyrins: Part 3 – Heavy-atom effects. J Chem Soc, Faraday Trans 2 1981;77:1281–1291.
35. Eastwood D, Gouterman M. Porphyrins XVIII. Luminescence of (Co), (Ni), Pd, Pt complexes. J Mol Spectrosc 1970;35:359–375.
36. Achord JM, Hussey CL. Determination of dissolved oxygen in nonaqueous electrochemical solvents. Anal Chem 1980;52:601–602.
37. Wilkinson WP, Helman WP, Ross AB. Quantum yields for the photosensitized formation of the lowest electronically excited singlet state of molecular oxygen in solution. J Phys Chem Ref Data 1993;22:113–262.
38. Redmond WR, Gamlin JN. A compilation of singlet oxygen yields from biologically relevant molecules. Photochem Photobiol 1999;70:391–475. [PubMed: 10546544]
39. Demas JN, Harris EW, McBride RP. Energy transfer from luminescent transition metal complexes to oxygen. J Am Chem Soc 1977;99:3547–3551.
40. Birks, JB. Photophysics of Aromatic Molecules. Wiley-Interscience; London: 1970. p. 492-517.
41. Gijzeman OLJ, Kaufman F, Porter G. Oxygen quenching of aromatic triplet states in solution. Part 1. J Chem Soc, Faraday Trans 2 1973;69:708–720.
42. Ware WR. Oxygen quenching of fluorescence in solution: an experimental study of the diffusion process. J Phys Chem 1962;66:455–458.
43. Kikuchi K, Kurabayashi Y, Kokubun H, Kaizu Y, Kobayashi H. Triplet yields of some tetraphenylporphyrins and octaethylporphyrins. J Photochem Photobiol A 1988;45:261–263.

44. Kajii Y, Obi K, Tanaka I, Tobita S. Isotope effects on radiationless transition from the lowest excited state of tetraphenylporphin. Chem Phys Lett 1984;111:347–348.
45. Bonnett R, McGarvey DJ, Harriman A, Land EJ, Truscott TG, Winfield UJ. Photophysical properties of meso-tetraphenylporphyrin and some meso-tetra(hydroxyphenyl)porphyrins. Photochem Photobiol 1988;48:271–276. [PubMed: 3222336]
46. Reindl S, Penzkofer A. Triplet quantum yield determination by picosecond laser double-pulse fluorescence excitation. Chem Phys 1996;213:429–438.
47. Posen Y, Kalchenko V, Seger R, Brandis A, Scherz A, Salomon Y. Manipulation of redox signaling in mammalian cells enabled by controlled photogeneration of reactive oxygen species. J Cell Sci 2005;118:1957–1969. [PubMed: 15840654]
48. Felton, RH. The Porphyrins. Dolphin, D., editor. Vol. V. Academic Press; New York: 1978. p. 5-125.
49. Gradyshko AT, Tsvirko MP. Probabilities for intercombination transitions in porphyrin and metalloporphyrin molecules. Opt Spectrosc 1971;31:291–295.
50. Hurley JK, Sinai N, Linschitz H. Actinometry in monochromatic flash photolysis: the extinction coefficient of triplet benzophenone and quantum yield of triplet zinc tetraphenyl porphyrin. Photochem Photobiol 1983;38:9–14.
51. Quimby DJ, Longo FR. Luminescence studies on several tetraarylporphins and their zinc derivatives. J Am Chem Soc 1975;97:5111–5117.
52. Callis JB, Gouterman M, Jones YM, Henderson BH. Porphyrins XXII: Fast fluorescence, delayed fluorescence, and quasiline structure in palladium and platinum complexes. J Mol Spectrosc 1971;39:410–420.

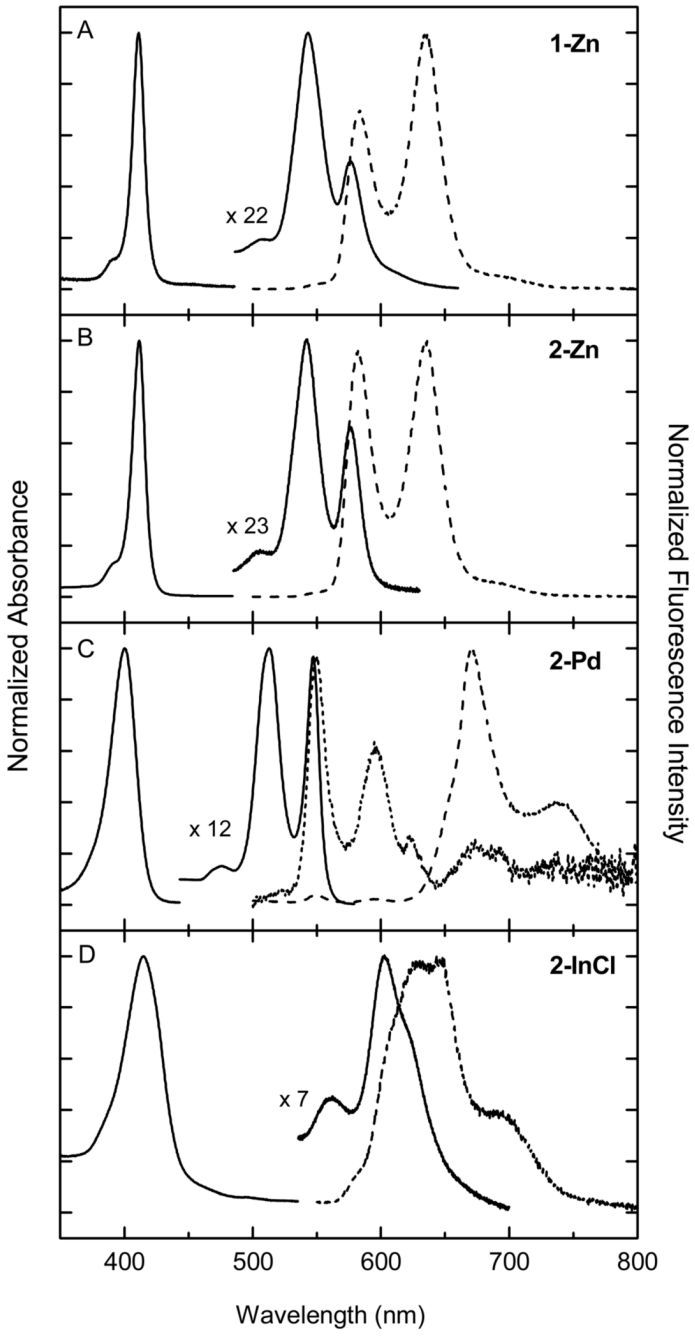

Fig. 1.

Absorption spectra (solid) and emission spectra (dashed for deoxygenated sample and dotted for oxygen-containing sample) for **2-Zn** (A), **1-Zn** (B), **2-Pd** (C), and **2-InCl** (D) in THF/MeOH (3:1) at room temperature.

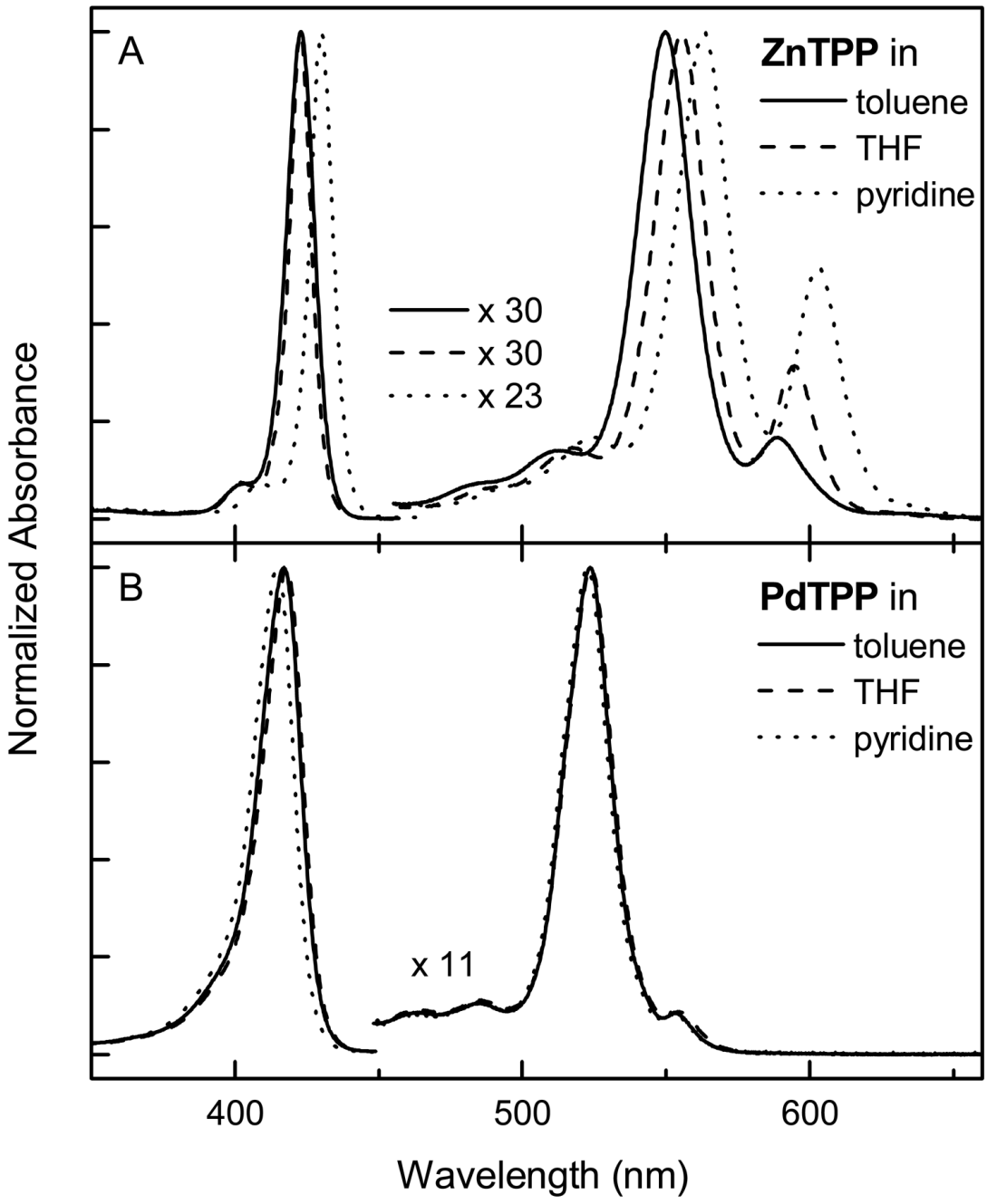

Fig. 2.
Absorption spectra of **ZnTPP** (A) and **PdTPP** (B) in toluene (solid), THF (dashed), and pyridine (dotted) at 295 K.

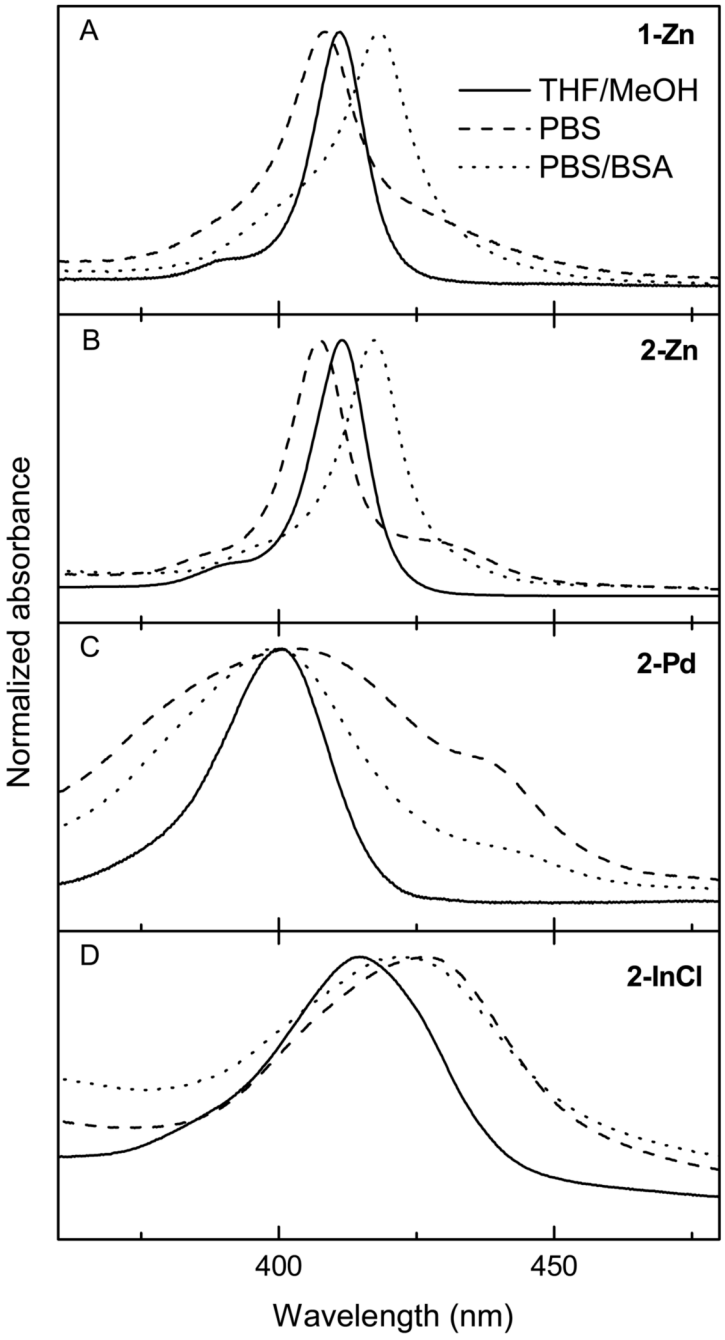

Fig. 3.
Room-temperature Soret-region absorption spectra of the metalloporphyrins in THF/MeOH (3:1) (solid), PBS (dashed), and PBS/BSA (dotted).

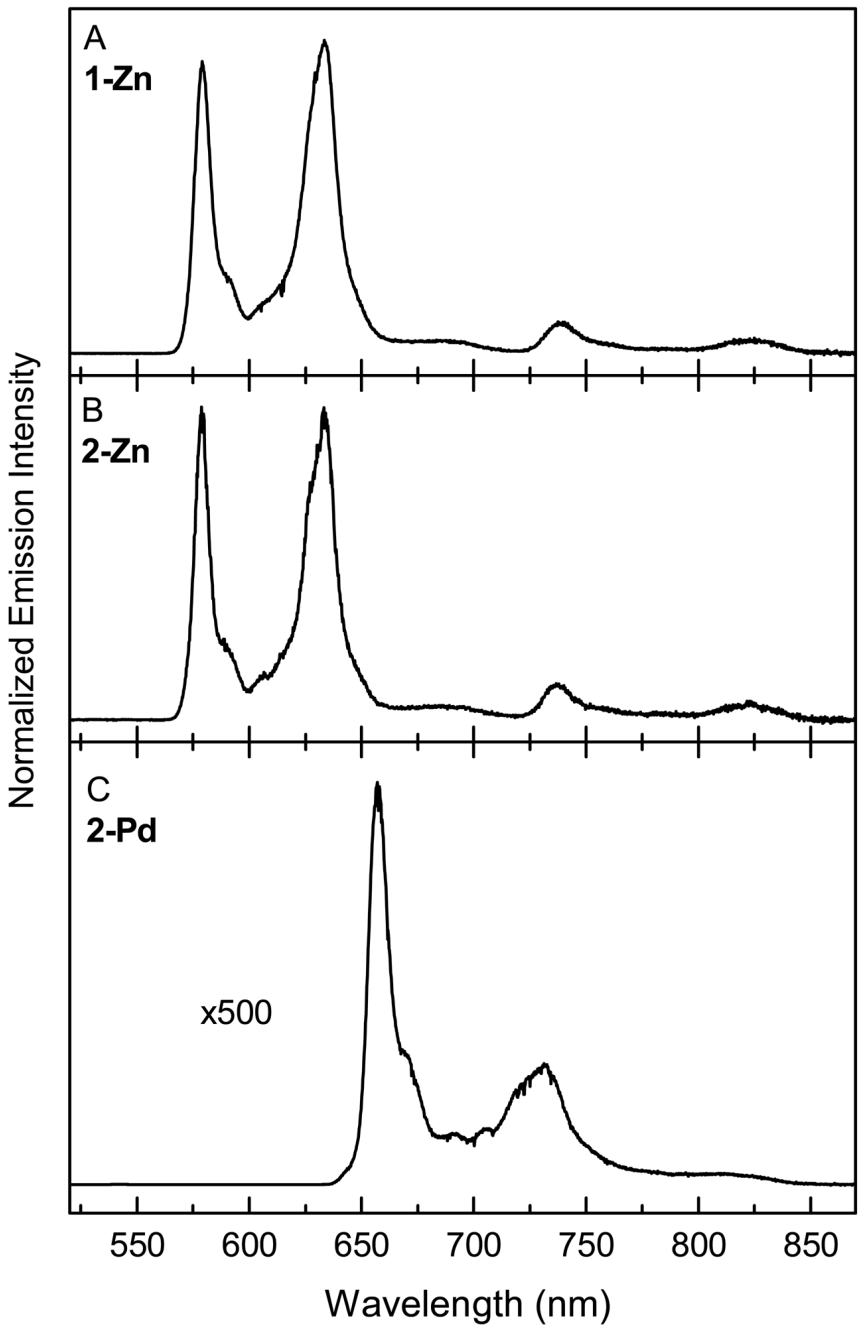

Fig. 4.

Emission spectra of the **2-Zn** (A), **1-Zn** (B), and **2-Pd** (C) in ethanol glass at 77 K. The features at wavelengths shorter than ~640 nm are from fluorescence and those to longer wavelengths are phosphorescence.

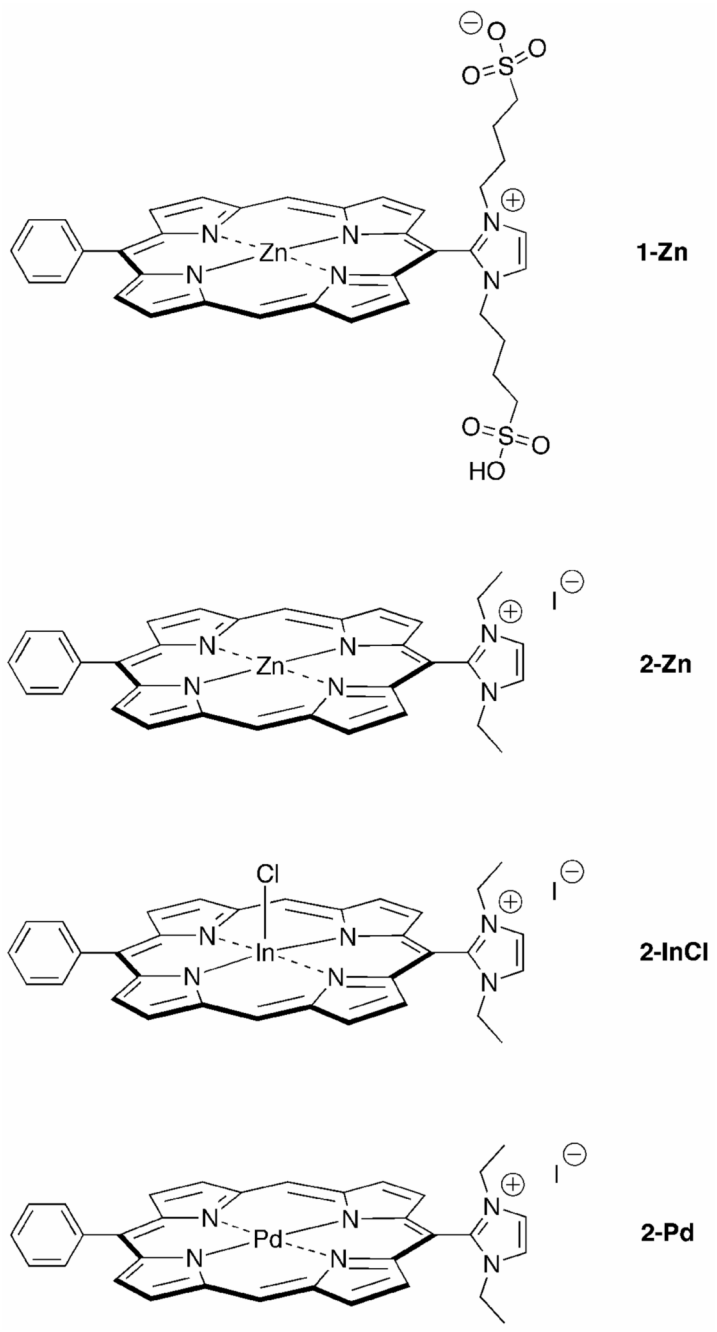

Chart 1.

Table 1

Absorption and fluorescence spectral properties at 295 K.

Cmpd	Medium	Absorption						Fluorescence	
		B(0,0) (nm)	B(0,0) FWHM (nm)	Q(1,0) (nm)	Q(0,0) (nm)	B(0, 0)/Q(1, 0)	B(0, 0)/Q(1, 0)	Q(0,0) (nm)	Q(0,1) (nm)
1-Zn	THF/MeOH	411	11	543	576	22	0.4	583	635
	cPBS	410		552	582			586	
	cPBS/BSA	419		552	582			594	
	PBS	408		547	579				
	PBS/BSA	418		550	581				
2-Zn	THF/MeOH	412	12	542	576	23	0.7	582	635
	cPBS	409		547	581			585	
	cPBS/BSA	418		549	580			593	
	PBS	407		541	575				
	PBS/BSA	417		547	579				
2-Pd	THF/MeOH	400	24	513	547	12	1.0	550	591
	cPBS	406		519	559			563	
	cPBS/BSA	400		517	555			563	
	PBS	403		518	558			562	
	PBS/BSA	399		517	555			552	
2-InCl	THF/MeOH	415	38	561	603	15	2.3	637	692
	cPBS	430		594	627				
	cPBS/BSA	428		597	627				
	PBS	426		597	626			638	
	PBS/BSA	422		595	624			628	
ZnTPP	toluene	423	11	550	589	30	0.16	596	646
	THF	423	9	555	594	30	0.31		
PdTPP	toluene	417	17	524	553	11	0.08	560	607
	THF	418	17	524	553	11	0.08		

J Photochem Photobiol A Chem. Author manuscript; available in PMC 2009 December 15.

Table 2

Summary of photophysical data.

Cmpd	T[a] (K)	Absorption B(0,0) (nm)	Absorption Q(0,0) (nm)	Emission Q(0,0) (nm)	Emission T(0,0) (nm)	E_S (eV)	E_T (eV)	$E_S E_T$ (eV)	Φ_p/Φ_f	τ_S (ns)	Φ_f	$(k_f)^{-1}$ (ns) [b]	Φ_{isc}	$(k_{isc})^{-1}$ (ns)[c]	$(k_{isc}^{ref})^{-1}$ (ns)[d]	Φ_{isc}^{ref}[a]	τ_T (ms)	Φ_p[f]	$(k_p)^{-1}$ (ms)
1-Zn	295	411	576	583		2.12				3.0[g]	0.014[h]	214[i]	0.69	4.3	3.7	0.80	4.5[j]		
	77			579	738	2.14	1.68	0.46	0.11								64	0.0015	33000
2-Zn	295	412	576	582		2.13				3.0[k]	0.015[l]	200[m]	0.79	3.8	3.8	0.80	6.1[j]		
	77			579	738	2.14	1.68	0.46	0.14								54	0.0021	21000
2-Pd	295	400	547	550	672	2.25	1.84	0.41	26	0.009	0.00012	75	0.88	0.010	0.009	>0.99	0.01[j]		
	77			542	657	2.28	1.89	0.39	650								2.0	0.078	26
2-InCl	295	415	603	637		1.95	1.50[n]	0.45		0.24	0.0078	31	0.83	0.29	0.25	0.98			
ZnTPP	295	423	588	595		2.08				2.1[o]	0.030[p]	70[q]	0.85[r]	2.5[s]		0.85	4.6		
	77			599	784	2.07	1.58	0.49	0.11[t]								33[u]	0.0033[v]	8500[w]
PdTPP	295	417	553	560	696	2.21	1.78	0.43	11	~ 0.01[x]	0.00018[y]			~0.01[z]			0.11		
	77				683		1.82		>460[aa]							>0.99	1.5[ab]	>0.08[ac]	<19

[a] Unless noted otherwise, studies on **1-Zn**, **2-Zn**, **2-Pd**, and **2-InCl** at 295 K utilized samples in MeOH/THF = 3:1, and studies at 77 K utilized samples in frozen ethanol glasses. Studies on **ZnTPP** and **PdTPP** utilized samples in toluene, except for determinations of τ_T, which used 2-MeTHF solutions (295 K) or frozen glasses (77 K).

[b] Calculated using Eq. (4).

[c] Calculated using Eq. (5).

[d] Calculated using Eq. (6) and the value of $k_{IC} = (16.2\ \text{ns})^{-1}$ for **ZnTPP**.

[e] Calculated using Eq. (7) and the value in the preceding column.

[f] Obtained by multiplying the Φ_p/Φ_f (obtained from the emission spectra at 77 K) times the value of Φ_f determined at 295 K, assuming that Φ_f is not affected substantially by temperature [29,[49]].

[g] The values in cPBS and cPBS/BSA are 2.5 ns and 2.7 ns, respectively.

[h] The values in cPBS and cPBS/BSA are 0.019 and 0.020, respectively.

[i] The values in cPBS and cPBS/BSA are $(132\ \text{ns})^{-1}$ and $(135\ \text{ns})^{-1}$, respectively.

[j] Compound in ethanol.

[k] The values in cPBS and cPBS/BSA are 2.6 ns and 2.7 ns, respectively.

[l] The values in cPBS and cPBS/BSA are 0.019 and 0.014, respectively.

[m] The values in cPBS and cPBS/BSA are $(136\ \text{ns})^{-1}$ and $(193\ \text{ns})^{-1}$, respectively.

[n] Obtained assuming an average value of $E_S - E_T = 3500\ \text{cm}^{-1}$ from **1-Zn**, **2-Zn**, and **2-Pd**.

[o] Measured in toluene in ref. [31]. A value of 2.2 ns is measured in toluene in ref. [49]. A value of 2.7 ns is measured in methylcyclohexane in ref. [34].

[p] Measured in toluene in refs. [22] and [49], and in methylcyclohexane in ref. [34].

[q] The same value is derived in ref. [49] and a value of 59 in ref. [34].

[r] Derived from the values obtained in ref. [50] (0.83) and here (0.9).

[s] A value of 2.8 ns is reported in ref. [34].

[t] Additional values are reported in refs. [49] (0.37) and [51] (0.32).

[u] Additional values are reported in refs. [49] (25) and [34] (26).

[v] Additional values are reported in refs. [34] (0.012) and [49] (0.015).

[w] Additional values are reported in refs. [49] (1700) and [34] (2000).

[x] Calculated as described in the text. A value of 0.02 ns near the instrument limit is reported in ref. [34].

[y] Averaged of values from refs. [52] (0.00015), [25] (0.0002), and [34] (0.0002).

[z] Calculated as described in the text. A value of 0.02 is derived in ref. [34].

[aa] No fluorescence is observed, so the ratio is calculated based on the phosphorescence intensity above the baseline.

[ab] Additional values are reported in refs. [35] (2.4) and [34] (2.8).

[ac] Additional values are reported in refs. [52] (0.08), [34] (0.17), and [35] (0.2).